Energy & Environmental Science

PAPER

View Article Online
View Journal | View Issue

Cite this: *Energy Environ. Sci.*, 2018, **11**, 641

Flexible crystalline silicon radial junction photovoltaics with vertically aligned tapered microwires†

Inchan Hwang, ‡[a] Han-Don Um, ‡[a] Byeong-Su Kim, [ab] Munib Wober[c] and Kwanyong Seo *[a]

Received 24th November 2017,
Accepted 17th January 2018

DOI: 10.1039/c7ee03340k

rsc.li/ees

Much attention has been paid to thin crystalline silicon (c-Si) photovoltaic devices due to their excellent flexibility characteristics, stable efficiency, and possibility of use as highly efficient next-generation flexible photovoltaic devices (FPVs). To fabricate thin c-Si FPVs, it is important to improve their light-absorption properties while maintaining the flexible characteristics. In this study, vertically aligned microwires (MWs) on a 50 μm-thick thin c-Si substrate are designed for novel FPVs. Increasing the length of the MWs enhances the optical properties of the thin c-Si without affecting its flexibility. To maximize the efficiency of the thin c-Si FPVs with MWs, tapered MWs and a localized back-contact structure are devised. This device shows a maximum efficiency of 18.9%. In addition, the proposed thin c-Si FPV with MWs shows high stability without any change in efficiency, even with 1000 bending cycles with a bending radius of 12 mm. Thus, we successfully demonstrate battery-free flexible electronic devices integrated with our thin c-Si FPVs with MWs.

Broader context

Flexible photovoltaics (FPVs) are one of the most promising research fields in the solar energy industry because they can be utilized as a continous power source for wearable and portable electronic devices. Thin crystalline silicon (c-Si) has attracted much attention as a potential means for FPVs because of its excellent flexibility while retaining the advantages of c-Si PVs of high efficiency and stability. For highly efficient thin c-Si FPVs, it is important to maximize light absorption while maintaining the flexibility characteristics. In general, the conventional c-Si photovoltaics have increased light absorption by applying surface structures. However, the surface structures without consideration of the flexibility would limit the flexibility of the FPVs because induced stress during bending cannot be uniformly dispersed. In this study, we fabricated FPVs based on a radial junction with vertically aligned tapered microwires on thin c-Si to realize highly efficient FPVs. We showed that tapered microwires are an ideal structure for highly efficient thin c-Si FPVs because these structures can maximize the light absorption without affecting the flexibility of the thin c-Si substrate. Our proposed flexible c-Si radial junction photovoltaics with vertically aligned tapered microwires that provide excellent photovoltaic performance and flexibility are expected to serve as a promising power system for wearable and portable applications.

Introduction

Portable electronics, designed for communication and entertainment, are rapidly expanding into our daily lives as they are incorporated into wearable devices such as wristwatches, bracelets, and eyewear.[1] Because of the drastically increased consumption of electrical power for portable and wearable devices, the integration of photovoltaic devices into such electronics has been extensively investigated to achieve a continuous power output.[2] Flexible photovoltaics (FPVs) have attracted considerable attention because they can be installed on the curved or bendable surfaces of portable electronics as a continuous power source.[3] Therefore, numerous studies have developed FPVs, including organic solar cells,[4] dye-sensitized solar cells,[5] and perovskite solar cells.[6] Despite tremendous efforts in improving FPVs, however, they have thus far exhibited efficiencies that are very modest in comparison with those of non-flexible crystalline silicon photovoltaics (c-Si PVs, 26.3%).[7,8] Although c-Si PVs with thick c-Si wafers (>200 μm) currently account for more than 90% of all PV market share due to

[a] *Department of Energy Engineering, Ulsan National Institute of Science and Technology (UNIST), Ulsan 44919, Republic of Korea. E-mail: Kseo@unist.ac.kr*
[b] *Department of Chemistry, Ulsan National Institute of Science and Technology (UNIST), Ulsan 44919, Republic of Korea*
[c] *John A Paulson School of Engineering and Applied Sciences, Harvard University, Cambridge, Massachusetts 02138, USA*

† Electronic supplementary information (ESI) available. See DOI: 10.1039/c7ee03340k

‡ These authors contributed equally to this work.

this material's abundance, high efficiency, and stability, it is difficult to make these wafers flexible because they tend to be fragile when an external force is applied.[7–9]

To overcome this issue, research has focused on developing thin c-Si PVs because they are projected to have high flexibility while retaining the advantages of c-Si PVs, such as high efficiency and stability.[3,9–16] It has been reported that thin c-Si wafers with a thickness of 50 μm can not only achieve the theoretical maximum efficiency (~29% power conversion efficiency) with no light-absorption loss, but also have high flexibility, with a bending radius ($R_{bending}$) of up to approximately 10 mm.[9,17] However, planar c-Si wafers with a thickness of less than 50 μm not only have a high surface reflectance over 30% but also absorption loss in the near-infrared (NIR) region due to the low light-absorption coefficient of c-Si, resulting in significant efficiency degradation.[15] One promising approach for realizing a highly efficient thin c-Si FPV involves the application of nanoscale or microscale structures, such as textured structures,[11,13,18,19] nanowires,[20,21] nanocones,[12,15,22] and hierarchical structures[23] to the surface. Although nanostructures show high light-absorption properties, nanostructured PVs have low quantum efficiency in the short-wavelength region because of recombination loss due to Auger recombination with a large doped surface area.[12,24] In contrast to nanostructures, vertically aligned microwires (MWs) with radial p–n junctions formed by core–shell structures are particularly attractive for achieving high-efficiency PV devices due to their excellent light-trapping and radial-junction effects.[25–30] Furthermore, the MWs are expected to be irrelevant to the flexible characteristics of thin c-Si regardless of their length during bending because of the gap-adjustment effect caused by the empty space between the wires.[31]

Here, as a simple structural strategy for these FPVs, we apply various lengths of vertically aligned MWs onto the thin c-Si FPVs (50 μm). The $R_{bending}$ value of the hybrid structure with various lengths (10–30 μm) of MWs positioned on the 50 μm-thick c-Si wafer is approximately 10 mm, regardless of the length of the MWs. Light absorption by the thin c-Si FPV with tapered MWs can be maximized by reducing the surface reflection to less than 2% by a gradual change of the effective refractive index.[32] Our best flexible device under optimized conditions exhibits a maximum power-conversion efficiency (PCE) of 18.9%. Furthermore, the thin c-Si FPV with tapered MWs maintains constant PV characteristics during up to 1000 repetitions of bending tests. This result shows that MW-based thin c-Si FPVs can be commercialized as highly efficient flexible solar cells. Thus, the use of MWs to construct an ideal hybrid structure on a thin c-Si wafer presents a unique opportunity for practically realizing highly stable and efficient FPVs.

Results and discussion

Flexibility characteristics of thin c-Si with MWs

The flexibility of c-Si strongly depends on its thickness. c-Si with a thickness of 50 μm shows high flexibility, with an $R_{bending}$ value of ~10 mm, indicating that thin c-Si wafers are promising for FPVs. For the thin c-Si, however, extremely low absorption of long-wavelength light occurs due to the low light-absorption coefficient of c-Si (6.4×10^1 cm^{-1} at a wavelength of 1000 nm). In addition, the planar thin c-Si substrate has high surface reflection, originating from impedance mismatching between air and the c-Si. To increase the light absorption of photovoltaics, random pyramidal structures have been employed for conventional c-Si PVs.[7] However, the random pyramidal structures formed on the thin c-Si intrinsically possess crack initiation sites under bending, as shown in Fig. S1a (ESI†). Due to the mechanical defects, the surface textured thin c-Si would be more easily broken when an external force is applied compared to the planar thin c-Si without the surface structures (Fig. S1b, ESI†). Therefore, a novel strategy is needed to improve light absorption while maintaining superior flexibility for the thin c-Si FPVs. In this study, we applied vertical Si MWs to a 50 μm-thick flexible c-Si substrate to improve its light-absorption characteristics. The vertically aligned MWs of lengths ranging from 10 to 30 μm were fabricated onto the thin c-Si substrates *via* photolithography and reactive ion-etching processes. The MWs have a regular hexagonal arrangement with a 2 μm diameter and a 2 μm gap between wires. To evaluate the flexibility of the thin c-Si as the MW length increases, an external force was applied to the samples using a bending tester, as shown in Fig. S2a (ESI†). The $R_{bending}$ was obtained by measuring the initial length of the sample ($L_{initial}$) without the external force and the changed length after applying the force, as follows:

$$R_{bending} = \frac{L_{initial}}{2\pi\sqrt{\frac{\Delta L}{L_{initial}} - \frac{\pi^2 h^2}{12 {L_{initial}}^2}}}$$

Here, $L_{initial}$, ΔL, and h represent the initial bending sample length, the change in sample length during the bending test, and the substrate thickness, respectively.[33] Fig. 1a shows the $R_{bending}$ values of planar c-Si with thicknesses ranging from 50 to 80 μm, as well as those of 50 μm-thick c-Si with vertically aligned MWs of lengths ranging from 10 to 30 μm. By increasing the thickness of the planar c-Si from 50 to 80 μm, $R_{bending}$ increased from 9.4 to 16 mm, showing that the thicker c-Si substrate has lower flexibility. The $R_{bending}$ values of the 50 μm-thick c-Si with vertically aligned MWs were almost consistent, falling in the range 9.4–9.75 mm. This indicates that the flexibility of thin c-Si with vertically aligned MWs depends only on c-Si thickness, rather than the MW length.

To elucidate the experimental results, we designed a thin c-Si structure for mechanical simulation, as shown in Fig. S2b (ESI†). The designed width and length of the thin c-Si were 60 and 700 μm, respectively, while the thickness was varied from 50 to 80 μm. The thin c-Si had one end fixed, such that the deflection at that end was zero. The deflection distance at the free end of c-Si under an applied stress of 200 N m^{-2} was numerically obtained using the following equation:

$$d = \frac{4\sigma L^3}{Et^2}$$

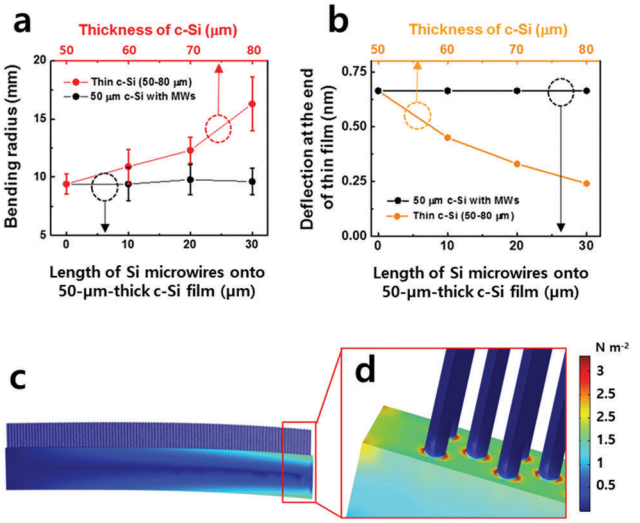

Fig. 1 (a) Experimental bending properties of various thicknesses of planar thin c-Si from 50 to 80 μm (red solid line with circles), as well as thin c-Si (50 μm) with various MW lengths from 0 to 30 μm (black solid line with circles). (b) Calculated deflection distances of various thicknesses of planar thin c-Si from 50 to 80 μm (orange solid line with circles) and simulated deflection distances of thin c-Si (50 μm) with various lengths of MWs from 0 to 30 μm (black solid line with circles) under an applied load of 200 N m^{-2}. (c and d) Stress distribution of thin c-Si with MWs.

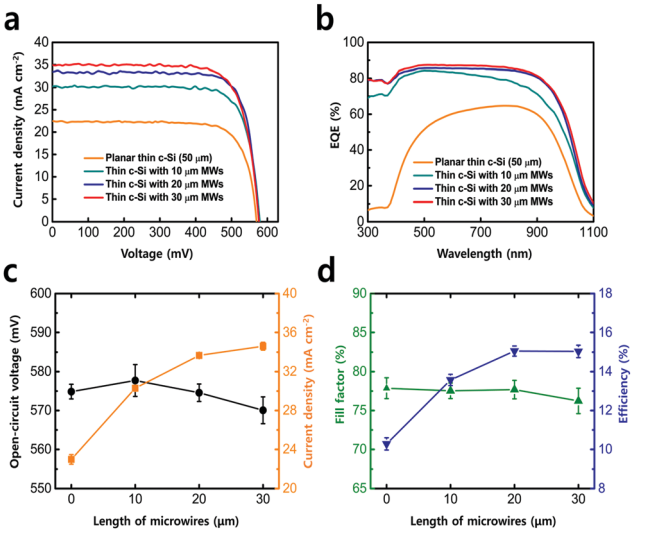

Fig. 2 (a) *J–V* characteristics and (b) EQE of the planar 50 μm-thick c-Si (orange solid line) and 50 μm-thick c-Si with various MW lengths: 10 μm (dark cyan solid line), 20 μm (blue solid line), and 30 μm (red solid line) under AM 1.5G illumination. (c) Open-circuit voltage (black solid line with circles) and short-circuit current density (orange solid line with squares). (d) Fill factor (green solid line with triangles) and efficiency (blue solid line with inverted triangles) extracted from the *J–V* curves plotted in Fig. 2a.

where d, σ, L, t, and E represent the deflection distance at the free end of the thin c-Si, applied stress, length, thickness of the thin c-Si, and Young's modulus of c-Si, respectively. The deflection distance increased with decreasing thickness of the thin c-Si (orange solid line with circles in Fig. 1b), indicating that thinner c-Si is more flexible. We also performed a finite-element method simulation (COMSOL, Multiphysics software package) of the mechanical characteristics of the thin c-Si with MWs. The deflection distances of the thin c-Si with MWs were consistent with the value for the 50 μm-thick c-Si without MWs, regardless of the MW length (black solid line with circles in Fig. 1b). This result can be explained by the regular stress distribution in the thin c-Si with MWs under a mechanical load, as shown in Fig. 1c and d. The induced stress was dispersed uniformly regardless of MW length when an external stress was applied to the thin c-Si substrate. These results demonstrate that the mechanical properties of thin c-Si with MWs are highly suitable for FPVs.

Characteristics of thin c-Si flexible PVs with MWs

By increasing the MW length, the light absorption of the thin c-Si can be improved owing to the reduced surface reflection and enhanced optical-path length due to multiple scattering of incident light (Fig. S3a and b, ESI†).[25] Fig. S3a (ESI†) shows the enhanced light absorption of the thin c-Si with increasing MW length. The integrated photon-flux absorption is an important factor because it can be used to estimate the theoretical current density (J_{sc}) of PV devices. The integrated photon-flux absorptions and theoretical J_{sc} values of each sample were calculated by the obtained absorption spectra (Fig. S3b, ESI†) with solar spectral photon-fluxes (AM 1.5G illumination) integrated over a wavelength range of 300–1100 nm (Fig. S3c, ESI†). The thin c-Si (50 μm) with 30 μm-long MWs showed an integrated photon-flux of 87% and a theoretical J_{sc} of 38.1 mA cm^{-2}, around 47% higher than that of the planar structure (integrated photon-flux = 59%; theoretical J_{sc} = 26.0 mA cm^{-2}).

We fabricated 50 μm-thick c-Si FPVs with MW lengths ranging from 10 to 30 μm. Fig. 2a shows the current density–voltage (*J–V*) curves of the thin c-Si FPVs with various MW lengths under AM 1.5G illumination. The PV parameters are summarized in Table 1. In Fig. 2a, the J_{sc} value obtained with 30 μm-long MWs is 34.6 mA cm^{-2}, representing a 51% improvement compared with the value for the planar devices (22.9 mA cm^{-2}). Although the values of J_{sc} in Fig. 2a are slightly lower than those predicted theoretically, due to recombination loss, we have confirmed the theoretical tendency of J_{sc} improvement with increased MW length. Fig. 2b shows the external-quantum-efficiency (EQE) of the thin c-Si FPVs with various MWs lengths. The EQE spectra of our devices were significantly improved over the entire wavelength range by increasing the MW length. In particular, the

Table 1 Average photovoltaic properties of thin c-Si (50 μm) FPVs with various lengths of MWs[a] (values in the brackets are obtained from the champion device)

Length of MWs	J_{sc} (mA cm^{-2})	V_{oc} (mV)	Fill factor (%)	Efficiency (%)
Planar c-Si (50 μm)	22.9 (23.4)	574 (577)	77.8 (78.7)	10.2 (10.6)
With 10 μm MWs	30.2 (30.3)	577 (581)	77.5 (78.2)	13.5 (13.8)
With 20 μm MWs	33.6 (34.1)	574 (576)	77.6 (77.3)	15.0 (15.2)
With 30 μm MWs	34.6 (35.2)	570 (567)	76.2 (77.6)	15.0 (15.2)

[a] Average photovoltaic performance for 10 devices.

EQE of the 30 μm-long MW device at a short wavelength of 300 nm showed a remarkably improved value of 78% compared to a value of 6.5% for the planar device. To clarify the enhancement of EQE in the short-wavelength region, the internal-quantum-efficiency (IQE) spectra were calculated using EQE and the reflectance spectra (Fig. S4, ESI†). The IQE value of the 30 μm-MW device (99%) was much higher than that of the planar device (27%) at a wavelength of 300 nm. This result can be explained by the outstanding light absorption property of the MWs and the radial-junction effect. Short-wavelength light was almost absorbed by the thin c-Si with MWs because of the high absorption coefficient of c-Si (*e.g.*, 173 μm^{-1} at a wavelength of 300 nm), as shown in Fig. S5a (ESI†). Considering the emitter-junction depth of 300 nm in Fig. S5b (ESI†), a radial-junction was successfully formed in the MWs with a diameter of 2 μm. The generated minority carriers in the MWs could be effectively separated by the short diffusion length in the radial-junction.

In Fig. 2c, the open-circuit voltage (V_{oc}) initially tends to increase with MW length up to 10 μm, but then slightly decreases. This can be explained by the relationship between V_{oc} and the light-generated current/reverse-saturation current:[34]

$$V_{oc} = \frac{k_B T}{q} \ln\left(\frac{J_L}{J_0} + 1\right)$$

Here, q, k_B, T, J_L, and J_0 refer to electron charge, Boltzmann's constant, temperature, light-generated current, and reverse-saturation current, respectively. For the thin c-Si FPV with 10 μm-long MWs, V_{oc} exhibited an increased value (577 mV) compared to that obtained for a planar device (570 mV), because of the increase in light-generated current from 22.9 to 30.2 mA cm^{-2}. Although the thin c-Si FPV with 30 μm-long MWs showed an increase to 34.6 mA cm^{-2} in light-generated current, the V_{oc} of this device slightly decreased to 570 mV due to the increased reverse-saturation current aggravated by the longer MWs (Fig. S6, ESI†). As shown in Fig. 2d, the maximum PCE of the c-Si FPV with MWs was 15.2% for the 20- and 30 μm-long MWs due to the trade-off between saturated J_{sc} and slightly decreased V_{oc} that occurred for longer MWs while maintaining a consistent $R_{bending}$ of ~10 mm.

Improved PV performance of thin c-Si FPVs with tapered MWs and a localized back contact (LBC)

As can be seen in Fig. 2c, the J_{sc} value of the c-Si FPVs with MWs becomes almost saturated around 34 mA cm^{-2} as the MW length increases from 20 to 30 μm. This result can be explained by the surface-reflection spectra of the thin c-Si with various MW lengths, as shown in Fig. S7a (ESI†). Although the length of the MWs increased by 200% from 20 to 40 μm, the surface reflection only decreased from 11.9% to 10.3%. This result was mainly due to the reflection of the flat-top-surface of the MWs, as shown in the inset of Fig. 3a. Because of the refractive-index mismatch between air (1) and Si (4), the incident light could have been reflected by the flat-top-surface area, which accounted for 24% of the top surface.[34] Consequently, the light absorption of the thin c-Si with MWs was not improved by increasing the MW length over 20 μm. To decrease the flat-top-surface reflection, a tapered-MW structure was fabricated using

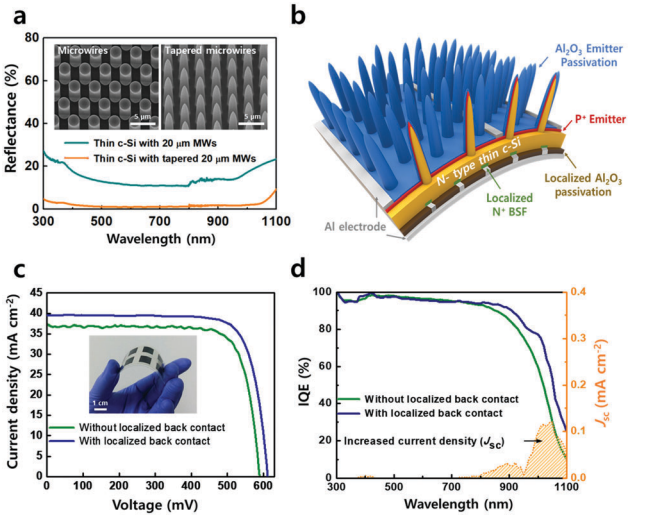

Fig. 3 (a) Reflection spectra for FPVs with tapered and non-tapered 20 μm-long MWs. (b) Schematic of the thin c-Si FPV with tapered MWs and LBC structure. (c and d) *J*–*V* and IQE curves of the tapered MW-based thin c-Si FPV with (blue solid line) and without localized back contact (green solid line) under AM 1.5G illumination.

a simple wet-etching process, as shown in the inset of Fig. 3a. When a thin c-Si wafer with MWs is dipped in a silicon etchant (RSE-100, transene), the top part of the MWs that has a shorter diffusion path compared to the bottom part is etched more quickly than the bottom part because of the different chemical-diffusion path lengths leading to the formation of tapered MWs. It was reported that tapered Si MWs with sharp top structures significantly reduced the surface reflection and increased broadband-light absorption.[35] Fig. 3a shows the surface reflection of the tapered and non-tapered MWs with lengths of 20 μm. Since the diameter of the tapered MWs gradually increased from the top to the bottom (Fig. S7b, ESI†), the tapered MWs can act as a buffer layer to compensate for the mismatch between the refractive indexes of air (1) and the silicon substrate (4). Thus, the surface reflection using the tapered MWs was observed to be less than 2% at a wavelength of 550 nm (Fig. S7c, ESI†). Due to the superior antireflection effect, the tapered MW-based FPV (37 mA cm^{-2}) exhibited a J_{sc} enhancement of 8.5% compared to that of the non-tapered-MW-based FPV (34 mA cm^{-2}).

The EQE of the thin c-Si FPV with tapered MWs was not improved over the 900 nm wavelength, even though tapered MWs significantly enhanced the light absorption of the thin c-Si wafer (Fig. S8a, ESI†). In this study, to form an ohmic contact and a back-surface field (BSF), a highly doped Si layer (n^+) was formed on the rear surface of the thin c-Si FPV, which was in full contact with the metal electrode. In practice, among the parts of a c-Si PV, the rear metal/semiconductor interface is the main source of NIR-recombination loss.[7] It has been reported that a localized back contact (LBC) structure can effectively increase the quantum efficiency of the NIR region by suppressing the rear-surface-recombination velocity (S_{eff}).[7,11] To increase the EQE response of the NIR-wavelength region, a LBC was fabricated on the rear side of the thin c-Si FPV with

Table 2 Improved photovoltaic properties of thin c-Si FPVs with tapered MWs caused by the localized back contact[a] (values in the brackets are obtained from the champion device)

	J_{sc} (mA cm^{-2})	V_{oc} (mV)	Fill factor (%)	Efficiency (%)
Without LBC	35.6 (37.0)	585 (586)	77.7 (77.5)	16.2 (16.8)
With LBC	39.3 (39.5)	603 (608)	76.3 (78.7)	18.1 (18.9)

[a] Average photovoltaic performance for 8 devices.

tapered MWs (Fig. 3b). As shown in Fig. S8b (ESI†), we confirmed that the LBC structure (67.8 cm s^{-1}) has a reduced S_{eff} value compared to that under the full-contact condition (310 cm s^{-1}). Fig. 3c shows the J–V curves of the tapered-MW-based thin c-Si FPV with and without the LBC. The FPV with the LBC had a significantly enhanced J_{sc} of 39.5 mA cm^{-2} compared to that of the FPV with a full-contacted rear side (37 mA cm^{-2}), as presented in Table 2. To clarify the effect of the LBC, Fig. 3d compares the internal quantum efficiency (IQE) spectra of the devices with and without the LBC. The IQE of the LBC-based device increased significantly in the NIR-wavelength region due to the reduced surface-recombination velocity at the rear side. Also, we verified that the enhanced J_{sc} values of the LBC-based flexible devices originate mainly from the increased IQE response in the NIR region in Fig. 3d. Moreover, the V_{oc} of the LBC device was substantially increased from 586 to 608 mV because of the reduced rear-side surface recombination. As a result, our fabricated thin c-Si FPV with tapered MWs showed a maximum efficiency of 18.9% by suppressing rear-side recombination. Compared with the previously reported FPVs, the proposed thin c-Si FPVs with tapered MWs exhibited higher efficiency (Fig. S9, ESI†).

Bending stability of thin c-Si FPVs with tapered MWs and the demonstration of a flexible solar-powered electronic device

The advantages of high flexibility and enhanced light-trapping efficiency suggest that the proposed thin c-Si FPV with tapered MWs is highly efficient. Thus, the PV properties of this FPV were measured through a bending test (Fig. 4a). The bending speed was 300 mm min^{-1}, and 1000 repetitions were performed. In the bending test, the curvature radius of the thin c-Si FPV with tapered MWs was limited to 12 mm due to the bending limitations of the 50 μm-thick substrate. However, the flexibility of our proposed FPVs can be enhanced by reducing the c-Si substrate thickness. As shown in Fig. 4b, all PV parameters including V_{oc}, J_{sc}, fill factor, and PCE remained constant during the bending test, indicating that our device has superior flexibility and does not sustain mechanical damage. In addition, we measured the J_{sc} value of our flexible device under different $R_{bending}$ values (Fig. S10, ESI†). The J_{sc} values were almost identical as $R_{bending}$ decreased due to the high aspect ratio of the MWs, which can effectively scatter and absorb the incident light with a broad incident-angle range.[36]

Because of the outstanding flexible and PV characteristics, our proposed FPV can be applied to curved and bendable surfaces for various portable applications. To demonstrate a solar-powered battery-free electronic watch, four thin c-Si FPVs

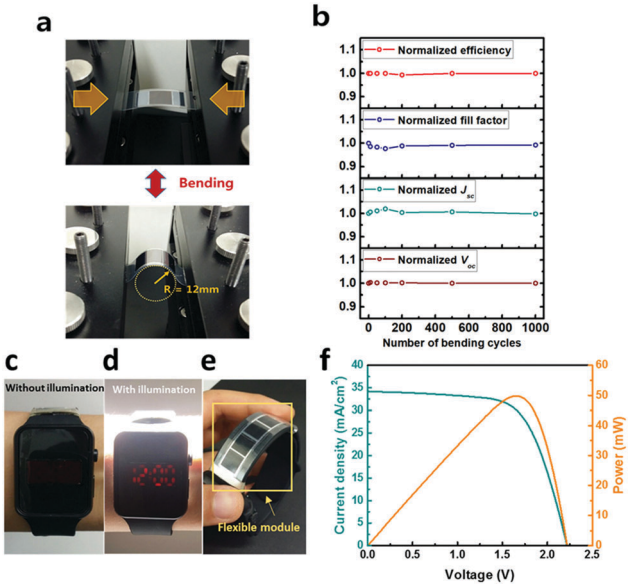

Fig. 4 (a) Pictures of the thin c-Si FPV with 20 μm-long tapered MWs before and after the bending test. (b) Normalized values of J_{sc} (dark cyan solid line with unfilled circles), V_{oc} (brown solid line with unfilled circles), fill factor (blue solid line with unfilled circles), and efficiency (red solid line with unfilled circles) as functions of bending cycle. (c) Pictures of solar-powered battery-free electronic watch without illumination and (d) with AM 1.5G illumination. (e) FPV module integrated into the electronic watch. (f) J–V (dark cyan solid line) and power–voltage (orange solid line) curves of the FPV module (all four flexible solar cells are connected in a series-active area of 4 cm^2). Under solar irradiation of AM 1.5G, our modules output 50 mW.

with tapered MWs were fabricated in series. Our flexible module (with an active area of 4 cm^2) showed a working voltage of 2.2 V and an output power of 50 mW (Fig. 4f). The flexible module was integrated onto the flexible strap of the battery-free electronic watch, as shown in Fig. 4e, which was successfully operated by integrating the flexible module of the thin c-Si FPV with tapered MWs (Fig. 4c–e and Supplementary video 1, ESI†). Also, we confirmed that our FPV could successfully power an electric fan under the bending test (Supplementary video 2, ESI†). Therefore, we anticipate that thin c-Si FPVs with tapered MWs can be integrated into flexible electronic appliances for the realization of solar-powered electronics.

Conclusions

We demonstrated the outstanding flexibility of the thin c-Si substrate with MWs. The experimental result showed that the $R_{bending}$ value of the thin (50 μm-thick) c-Si substrate with MWs was approximately 10 mm, regardless of the MW length. In addition, we confirmed through mechanical simulation that the bending stress only affects the thin c-Si substrate and the local interface between MWs and the substrate, regardless of the MW length. To maximize the light absorption of the thin c-Si FPV, tapered MWs were devised using a simple wet-etching process, and this structure showed an extremely low surface reflection below 2% when the impedance mismatch between air and Si was reduced. As a result, we achieved a thin c-Si FPV

with a remarkable efficiency of 18.9% by applying the tapered MWs and LBC to the thin c-Si FPV. Our thin c-Si FPV with tapered MWs showed stable PV properties without any changes in J_{sc}, V_{oc}, or fill factor, even after 1000 repetitions of the bending test. In addition, we demonstrated a solar-powered electronic device by integrating the thin c-Si FPVs with tapered MWs into an electronic watch. Therefore, our proposed thin c-Si structure with tapered MWs is expected to be a highly efficient and flexible PV device that can be integrated with flexible electronics.

Experimental

Fabrication of microwires (MWs) on the thin crystalline Si (c-Si) wafer

Czochralski (Cz) grade n-type c-Si wafers (resistivity of 1–3 Ω cm, 380 μm-thick) were etched by 80 °C KOH etching solution to fabricate thin c-Si substrates. The etching mask of photoresist dot arrays (2 μm in diameter, 2 μm spacing) was periodically patterned on the thin c-Si substrates using an AZ-nLOF-2035 photoresist (AZ Electronic Materials) by the photolithography process. The patterned thin c-Si substrates were etched by the deep reactive ion etching (DRIE, Tegal 200) process with 1500 W source power, 100 W stage power, and 45 mTorr gas pressure under source gases of SF_6 (250 sccm) and C_4F_8 (150 sccm).

Fabrication of thin c-Si flexible photovoltaics (FPV) with MWs

The emitter and the back-surface-field (BSF) layers were formed by using the spin-on-dopant (SOD) method. First, a phosphorus source (P509, Filmtronics, Inc.) was spin-coated on a dummy Si wafer, and then baked at 200 °C for 20 min to remove the organic solvent. The rear side of the thin c-Si substrate was positioned to face the P509 coated dummy wafer to form a BSF layer. The diffusion doping was carried out in a tube furnace under a mixed atmosphere of O_2 (125 sccm) and N_2 (500 sccm) at 900 °C. Phosphorus silicate glass that formed after the SOD diffusion process was removed by buffered oxide etchant (BOE). After removing phosphorus silicate glass, an emitter layer was formed by using a boron source (B155, Filmtronics, Inc.). The B155 solution was spin-coated on a dummy Si wafer, and then baked at 200 °C for 20 min. To form the conformal emitter layer on the MWs, the thin c-Si substrate with MWs was positioned to face the B155 coated dummy wafer. The diffusion doping process was carried out in a tube furnace under 500 sccm N_2 at 880 °C. A thin Al_2O_3 layer (10 nm-thick) used as a passivation layer was deposited by using atomic layer deposition (Lucida D100, NCD). To fabricate the top-microgrid electrode, the front surface of the thin c-Si FPV with MWs was patterned by the photolithography process using an AZ4330 photoresist (AZ electronic materials). For the top and bottom electrodes, 500 and 200 nm-thick Al films were deposited on the top and bottom of samples using the e-beam evaporator (Temescal), respectively. Finally, the photoresist residue was removed by acetone solution. The active area of the fabricated FPV was 1 cm^2.

Fabrication of thin c-Si FPV with tapered MWs and localized back contact (LBC)

To fabricate tapered MWs on the thin c-Si substrate, the thin c-Si with MWs was immersed in slow silicon etchant (RSE-100) for 10 s. A SiO_2 layer of 300 nm was deposited on the rear side of the thin c-Si with tapered MWs by using plasma-enhanced chemical vapor deposition (PE-CVD, PEH-600). The localized back contact on the rear side of samples was patterned by photolithography using the AZ4330 photoresist (AZ electronic materials). The localized BSF layer was formed in a tube furnace under a mixed atmosphere of O_2 (125 sccm) and N_2 (500 sccm) at 900 °C by using the P509 dopant source. After the formation of a localized BSF layer, the emitter layer was formed on the top surface of the thin c-Si with tapered MWs under a mixed atmosphere of N_2 (500 sccm) at 880 °C by using the B155 dopant source. The Al_2O_3 passivation layer of 10 nm was deposited on the front and rear sides of the thin c-Si with tapered MWs using atomic layer deposition (Lucida D100, NCD). The top micro-gird was patterned by the photolithography process. For the top and bottom electrodes, 500 and 200 nm-thick Al films were deposited on the top microgrid and bottom localized BSF layer using the e-beam evaporator (Temescal), respectively. The active area of the fabricated solar cells was 1 cm^2.

Photovoltaic characterization

The photovoltaic properties of solar cells were tested using an Oriel Sol3A Class AAA solar simulator (Newport) under AM 1.5G illumination. Incident flux was confirmed by a calibrated power meter, and double-checked using a NREL-calibrated solar cell (PV Measurements, Inc.). The EQE spectra were measured using a Xe light source and a monochromator with a wavelength range of 300–1100 nm. Optical reflections of samples were measured *via* a UV-Vis-NIR spectrophotometer (Cary 5000, Agilent) equipped with a 110 mm integrating sphere to account for total light (diffuse and specular) reflected from the samples.

Bending test

To evaluate the mechanical flexibility of the thin c-Si FPV with tapered MWs, a custom-made bending test system was used to determine the efficiency characteristics of the flexible devices.

Author contribution

K. S. conceived the idea. I. H., H. U., M. W. and K. S. designed the experiment. I. H. and H. U. carried out the device fabrication, photovoltaic characterization and analysis. M. W. carried out the mechanical simulation. B. K. helped in the bending test of the device. I. H., H. U. and K. S. wrote the paper and all other authors commented on the manuscript.

Conflicts of interest

There are no conflicts to declare.

Acknowledgements

This work was supported by the National Research Foundation of Korea (NRF) grant funded by the Korea government (MSIP) (NRF-2017R1A2B4002738 & 2015R1D1A1A01059726).

References

1 M. J. Cima, *Nat. Biotechnol.*, 2014, **32**, 642–643.
2 H.-D. Um, K.-H. Choi, I. Hwang, S.-H. Kim, K. Seo and S.-Y. Lee, *Energy Environ. Sci.*, 2017, **10**, 931–940.
3 M. Pagliaro, R. Ciriminna and G. Palmisano, *ChemSusChem*, 2008, **1**, 880–891.
4 J. H. Seo, H.-D. Um, A. Shukla, I. Hwang, J. Park, Y.-C. Kang, C. S. Kim, M. Song and K. Seo, *Nano Energy*, 2015, **16**, 122–129.
5 K. Yoo, J.-Y. Kim, J. A. Lee, J. S. Kim, D.-K. Lee, K. Kim, J. Y. Kim, B. Kim, H. Kim, W. M. Kim, J. H. Kim and M. J. Ko, *ACS Nano*, 2015, **9**, 3760–3771.
6 D. Yang, R. Yang, J. Zhang, Z. Yang, S. Liu and C. Li, *Energy Environ. Sci.*, 2015, **8**, 3208–3214.
7 C. Battaglia, A. Cuevas and S. De Wolf, *Energy Environ. Sci.*, 2016, **9**, 1552–1576.
8 P.-J. Ribeyron, *Nat. Energy*, 2017, **2**, 17067.
9 A. W. Blakers and T. Armour, *Sol. Energy Mater. Sol. Cells*, 2009, **93**, 1440–1443.
10 G. P. Willeke, *Sol. Energy Mater. Sol. Cells*, 2002, **72**, 191–200.
11 M. S. Branham, W. C. Hsu, S. Yerci, J. Loomis, S. V. Boriskina, B. R. Hoard, S. E. Han and G. Chen, *Adv. Mater.*, 2015, **27**, 2182–2188.
12 S. Jeong, M. D. McGehee and Y. Cui, *Nat. Commun.*, 2013, **4**, 2950.
13 A. Mavrokefalos, S. E. Han, S. Yerci, M. S. Branham and G. Chen, *Nano Lett.*, 2012, **12**, 2792–2796.
14 J. H. Petermann, D. Zielke, J. Schmidt, F. Haase, E. G. Rojas and R. Brendel, *Prog. Photovoltaics*, 2012, **20**, 1–5.
15 S. Wang, B. D. Weil, Y. Li, K. X. Wang, E. Garnett, S. Fan and Y. Cui, *Nano Lett.*, 2013, **13**, 4393–4398.
16 K. J. Yu, L. Gao, J. S. Park, Y. R. Lee, C. J. Corcoran, R. G. Nuzzo, D. Chanda and J. A. Rogers, *Adv. Energy Mater.*, 2013, **3**, 1401–1406.
17 T. Tiedje, E. Yablonovitch, G. D. Cody and B. G. Brooks, *IEEE Trans. Electron Devices*, 1984, **31**, 711–716.
18 C.-C. Lin, Y.-J. Chuang, W.-H. Sun, C. Cheng, Y.-T. Chen, Z.-L. Chen, C.-H. Chien and F.-H. Ko, *Microelectron. Eng.*, 2015, **145**, 128–132.
19 Q. Lin, D. Sarkar, Y. Lin, M. Yeung, L. Blankemeier, J. Hazra, W. Wang, S. Niu, J. Ravichandran, Z. Fan and R. Kapadia, *ACS Nano*, 2017, **11**, 5113–5119.
20 M. Sharma, P. R. Pudasaini, F. Ruiz-Zepeda, D. Elam and A. A. Ayon, *ACS Appl. Mater. Interfaces*, 2014, **6**, 4356–4363.
21 M. D. Ko, T. Rim, K. Kim, M. Meyyappan and C. K. Baek, *Sci. Rep.*, 2015, **5**, 11646.
22 Y. Mi, L. Wen, R. Xu, Z. Wang, D. Cao, Y. Fang and Y. Lei, *Adv. Energy Mater.*, 2016, **6**, 1501496.
23 H.-P. Wang, T.-Y. Lin, C.-W. Hsu, M.-L. Tsai, C.-H. Huang, W.-R. Wei, M.-Y. Huang, Y.-J. Chien, P.-C. Yang, C.-W. Liu, L.-J. Chou and J.-H. He, *ACS Nano*, 2013, **7**, 9325–9335.
24 J. Oh, H.-C. Yuan and H. M. Branz, *Nat. Nanotechnol.*, 2012, **7**, 743–748.
25 S.-H. Baek, H. S. Jang and J. H. Kim, *Curr. Appl. Phys.*, 2011, **11**, S30–S33.
26 R. Elbersen, W. Vijselaar, R. M. Tiggelaar, H. Gardeniers and J. Huskens, *Adv. Energy Mater.*, 2016, **6**, 1501728.
27 Y. Li, Q. Chen, D. He and J. Li, *Nano Energy*, 2014, **7**, 10–24.
28 M. C. Putnam, S. W. Boettcher, M. D. Kelzenberg, D. B. Turner-Evans, J. M. Spurgeon, E. L. Warren, R. M. Briggs, N. S. Lewis and H. A. Atwater, *Energy Environ. Sci.*, 2010, **3**, 1037.
29 K. Seo, Y. J. Yu, P. Duane, W. Zhu, H. Park, M. Wober and K. B. Crozier, *ACS Nano*, 2013, **7**, 5539–5545.
30 W. Vijselaar, R. Elbersen, R. M. Tiggelaar, H. Gardeniers and J. Huskens, *Adv. Energy Mater.*, 2017, **7**, 1601497.
31 C. Y. Jiang, X. W. Sun, K. W. Tan, G. Q. Lo, A. K. K. Kyaw and D. L. Kwong, *Appl. Phys. Lett.*, 2008, **92**, 143101.
32 J. Zhu, Z. Yu, G. F. Burkhard, C.-M. Hsu, S. T. Connor, Y. Xu, Q. Wang, M. McGehee, S. Fan and Y. Cui, *Nano Lett.*, 2009, **9**, 279–282.
33 S.-I. Park, J.-H. Ahn, X. Feng, S. Wang, Y. Huang and J. A. Rogers, *Adv. Funct. Mater.*, 2008, **18**, 2673–2684.
34 K. Lee, I. Hwang, N. Kim, D. Choi, H. D. Um, S. Kim and K. Seo, *Nanoscale*, 2016, **8**, 14473–14479.
35 S. Yalamanchili, H. S. Emmer, K. T. Fountaine, C. T. Chen, N. S. Lewis and H. A. Atwater, *ACS Photonics*, 2016, **3**, 1854–1861.
36 M. D. Kelzenberg, S. W. Boettcher, J. A. Petykiewicz, D. B. Turner-Evans, M. C. Putnam, E. L. Warren, J. M. Spurgeon, R. M. Briggs, N. S. Lewis and H. A. Atwater, *Nat. Mater.*, 2010, **9**, 239–244.